



HAL
open science

Stability in water and electrochemical properties of the $\text{Na}_3\text{V}_2(\text{PO}_4)_2\text{F}_3 - \text{Na}_3(\text{VO})_2(\text{PO}_4)_2\text{F}$ solid solution

Long H. B. Nguyen, Thibault Broux, Paula Sanz Camacho, Dominique Denux, Lydie Bourgeois, Stéphanie Belin, Antonella Iadecola, François Fauth, Dany Carlier-Larregaray, Jacob Olchowka, et al.

► To cite this version:

Long H. B. Nguyen, Thibault Broux, Paula Sanz Camacho, Dominique Denux, Lydie Bourgeois, et al.. Stability in water and electrochemical properties of the $\text{Na}_3\text{V}_2(\text{PO}_4)_2\text{F}_3 - \text{Na}_3(\text{VO})_2(\text{PO}_4)_2\text{F}$ solid solution. *Energy Storage Materials*, 2019, 20, pp.324-334. 10.1016/j.ensm.2019.04.010 . hal-02172143

HAL Id: hal-02172143

<https://hal.science/hal-02172143>

Submitted on 3 Jul 2019

HAL is a multi-disciplinary open access archive for the deposit and dissemination of scientific research documents, whether they are published or not. The documents may come from teaching and research institutions in France or abroad, or from public or private research centers.

L'archive ouverte pluridisciplinaire **HAL**, est destinée au dépôt et à la diffusion de documents scientifiques de niveau recherche, publiés ou non, émanant des établissements d'enseignement et de recherche français ou étrangers, des laboratoires publics ou privés.

Stability in water and electrochemical properties of the $\text{Na}_3\text{V}_2(\text{PO}_4)_2\text{F}_3 - \text{Na}_3(\text{VO})_2(\text{PO}_4)_2\text{F}$ solid solution

Long H. B. Nguyen^{a,b,g}, Thibault Broux^{a,b,h}, Paula Sanz Camacho^{a,g}, Dominique Denux^a, Lydie Bourgeois^{c,d}, Stéphanie Belin^e, Antonella Iadecola^g, François Fauth^f, Dany Carlier^{a,g}, Jacob Olchowka^{a,g}, Christian Masquelier^{b,g,h}, and Laurence Croguennec^{a,g,h}¹

^a CNRS, Univ. Bordeaux, Bordeaux INP, ICMCB UMR 5026, F-33600, Pessac, France.

^b Laboratoire de Réactivité et de Chimie des Solides, CNRS-UMR# 7314, Université de Picardie Jules Verne, F-80039 Amiens Cedex 1, France.

^c Univ. Bordeaux, ISM, Groupe de Spectroscopie Moléculaire, F-33405 Talence, France

^d Bordeaux INP, ISM, CNRS UMR 5255, F-33405 Talence, France

^e SOLEIL Synchrotron, F-91192 Gif-sur-Yvette, France.

^f CELLS-ALBA synchrotron, E-08290 Cerdanyola del Vallès, Barcelona, Spain.

^g RS2E, Réseau Français sur le Stockage Electrochimique de l'Energie, FR CNRS 3459, F-80039 Amiens Cedex 1, France.

^h ALISTORE-ERI European Research Institute, FR CNRS 3104, Amiens, F-80039 Cedex 1, France.

Abstract

Polyanionic materials have been intensively studied as promising active materials for positive electrodes in Na-ion batteries thanks to their excellent stability upon cycling and the fast ionic mobility in their structural framework. Among them, $\text{Na}_3\text{V}_2(\text{PO}_4)_2\text{F}_3$ and $\text{Na}_3(\text{VO})_2(\text{PO}_4)_2\text{F}$ are two of the most promising ones due to their high voltages for Na^+ -ion extraction and their high energy densities: 500 Wh.kg^{-1} and 495 Wh.kg^{-1} , respectively. Here, we study the formation mechanism as well as the stability of these phases in aqueous media and the possible use of a washing step in water in order to remove undesirable impurities formed during the synthesis. Furthermore, the origin of the extra capacity observed in the high voltage region for $\text{Na}_3\text{V}_2(\text{PO}_4)_2\text{F}_3$ and $\text{Na}_3\text{V}_2(\text{PO}_4)_2\text{F}_{1.5}\text{O}_{1.5}$ was studied by *operando* X-ray absorption spectroscopy.

¹ Corresponding author : L. Croguennec (Laurence.Croguennec@icmcb.cnrs.fr)

1. Introduction

Lithium-ion batteries (LIBs) are currently the most widely used technologies to power devices such as mobile phones, portable tools and laptops [1]. However, the unequal distribution of lithium resources in the earth's crust together with the booming electric vehicle market have raised several concerns about the stable supply and the cost of LIBs in the future. First introduced in the 1980s, the idea of developing Sodium-ion batteries (SIBs) remained poorly explored in the following years due to the striking development of LIBs. More recently, concerns on lithium resources conjugated to the accumulation of fundamental knowledge in the fields of SIBs lead to a resurgent interest in SIBs, expected to be used as an alternative next to LIBs so as to fulfill the constant increasing demand of energy storage devices [2]. A large panel of materials among layered oxides and polyanionic materials have been already explored as positive electrode materials for SIBs, such as: Na_xCoO_2 (126 mAh.g^{-1}) [3,4], $\text{Na}_3\text{V}_2(\text{PO}_4)_3$ (117.6 mAh.g^{-1}) [5,6], $\text{Na}_3\text{V}_2(\text{PO}_4)_2\text{F}_3$ (NVPF, 120 mAh.g^{-1}) [7–9] and very recently $\text{Na}_4\text{MnV}(\text{PO}_4)_3$ (156 mAh.g^{-1}) [10–12]. Among them, NVPF appears as the most promising one thanks to its high reversible capacity at high rates, and to its good stability [9]. The French Company TIAMAT is currently developing its Na-ion battery technology with NVPF at the positive electrode.

In the literature, it has been reported that $\text{Na}_3\text{V}^{3+}_2(\text{PO}_4)_2\text{F}_3$ and $\text{Na}_3(\text{V}^{4+}\text{O})_2(\text{PO}_4)_2\text{F}$ are the two end members of a series of $\text{Na}_3\text{V}_2(\text{PO}_4)_2\text{F}_{3-y}\text{O}_y$ compositions ($0 \leq y \leq 2$), the Na^+ extraction voltage being strongly dependent on the oxygen content [7,13,14]. These materials can be prepared via several synthesis routes: ceramic route, sol-gel, solvothermal, spray drying, co-precipitation ... [7,13–18]. However, the as prepared $\text{Na}_3\text{V}_2(\text{PO}_4)_2\text{F}_3$ powder often contains traces of impurities (Na_3VF_6 , $\text{Na}_5\text{P}_3\text{O}_{10}$...) that can be removed by washing at room temperature in a large excess of water [15]. In this paper, we first revisit and clarify the synthesis reaction that some of us proposed earlier [14]. The stability of $\text{Na}_3\text{V}_2(\text{PO}_4)_2\text{F}_{3-y}\text{O}_y$ -type materials in water is then addressed in order to determine if water-based electrode formulations are possible. Finally, we investigate the electrochemical mechanism occurring at high voltage as a function of the oxygen content in $\text{Na}_3\text{V}_2(\text{PO}_4)_2\text{F}_{3-y}\text{O}_y$.

Experimental

1.1.Synthesis procedures

A series of $\text{Na}_3\text{V}_2(\text{PO}_4)_2\text{F}_{3-y}\text{O}_y$ materials was prepared by a one-step solid-state reaction using stoichiometric amounts of VOPO_4 , VPO_4 , NaF (Sigma-Aldrich; $\geq 99\%$), and Na_2CO_3 (Riedel-de Haën; 99.8%). VPO_4 and VOPO_4 powders were obtained by using the stoichiometric reaction between V_2O_5 (Sigma-Aldrich; $\geq 99.6\%$) and $\text{NH}_4\text{H}_2\text{PO}_4$ (Sigma-Aldrich; $\geq 99.99\%$) as described in details earlier [14]. No coating with carbon was done, in order to better control the average oxidation state of vanadium in the samples. The as-prepared $\text{Na}_3\text{V}_2(\text{PO}_4)_2\text{F}_{3-y}\text{O}_y$ powders were washed in distilled water over four days in order to eliminate the impurities formed during the synthesis. The products were then filtered, and finally dried in a Buchi furnace at $80\text{ }^\circ\text{C}$ [14]. An optimized carbon-coated $\text{Na}_3\text{V}_2(\text{PO}_4)_2\text{F}_3$ material was used as a reference, the synthesis of which being described in details in a recently accepted patent [19].

1.2.Materials characterization

Thermogravimetric analyses were performed on a TGA Setaram TAG 2400 coupled with a mass spectrometer Balzer ThermoStar to identify the chemical compounds released by each sample during the thermal treatment. The experiments were carried out under Ar (alpha1) at a heating rate of $5\text{ }^\circ\text{C}\cdot\text{min}^{-1}$. Special care was taken to work with the best gas quality in order to increase the reproducibility of both the sample surrounding and the signals in mass spectrometry during the whole analysis.

Laboratory X-ray powder diffraction (XRPD) was carried out using a PANalytical Empyrean diffractometer in θ - θ configuration and equipped with a $\text{Cu K}_{\alpha 1,2}$ X-ray source. The powder was packed in a 0.5 mm diameter capillary. The acquisition was performed in the 2θ range of $8^\circ - 140^\circ$ with a step size of 0.004° . High angular resolution synchrotron powder X-ray diffraction (SPXRD) was performed at the MSPD beamline at ALBA (Barcelona, Spain). The data were recorded by using a MYTHEN detector at a wavelength of 0.8251 \AA , in the 2θ angular range of $1^\circ - 70^\circ$ with a 0.006° step. Diffraction data analysis and Rietveld refinements were performed by utilizing the FullProf Suite and Jana 2006 software [20,21]. The 3D crystal structure of the materials were visualized by using the VESTA software [22].

The chemical analysis of the Na, V, and P contents was performed by inductively coupled plasma-optical emission spectroscopy (ICP-OES) using a Varian Model 720-ES

spectrometer, after a complete dissolution of the powders into a concentrated hydrochloric acid (HCl) solution.

Scanning electron microscopy (SEM) images were taken on the metallized samples (Pd-deposited) by a Hitachi Model S-4500 microscope.

Fourier transform infrared (FT-IR) spectra were recorded by using a Bruker Equinox 55 spectrometer in the wavenumber range of 400 - 4000 cm^{-1} (mid-IR) with a resolution of 4 cm^{-1} . The samples were finely ground in a mortar with dried KBr in an approximate ratio of 1:50 (by wt.%).

^{23}Na solid-state NMR (ss-NMR) spectra were acquired using a Bruker Avance 500 MHz spectrometer, equipped with a 11.7 T widebore magnet (operating at Larmor frequency of 132.3 MHz for ^{23}Na). Experiments were performed using conventional 2.5 mm magic-angle spinning (MAS) probes, with 30 kHz MAS rate. Chemical shifts are references relative to an aqueous 0.1M NaCl solution at 0 ppm. In each case, a short pulse length of 1.1 μs corresponding to a selective $\pi/8$ pulse determined by using a 0.1 M NaCl aqueous solution was employed. The spectral width was set to 1 MHz and the recycle delay to 0.5 s, which was long enough to avoid T_1 saturation effects. The baseline distortions resulting from the spectrometer dead time (5–10 μs) were removed computationally by using a polynomial baseline correction routine. ^{31}P ss-NMR spectra were acquired on a Bruker Avance III 100 MHz spectrometer, equipped with a 2.4 T widebore magnet (operating at Larmor frequency of 40.6 MHz for ^{31}P) by using a standard Bruker 2.5 mm MAS probe at 30 kHz MAS rate. Chemical shifts are references relative to an aqueous H_3PO_4 85% (Sigma-Aldrich) solution at 0 ppm. In each case, a Hahn echo sequence was used with a $\pi/2$ pulse of 1.1 μs and a recycle delay of 0.2 s.

Synchrotron X-ray absorption spectroscopy (XAS) was performed at the Vanadium K-edge energy in transmission mode at the ROCK beamline of the SOLEIL synchrotron facility (Saint-Aubin, France). The storage ring was operated in multibunch top-up at 2.75 GeV with a 450 mA current. The incident beam from the bending magnet was collimated and horizontally focusing by a first toroidal bendable silicon Ir coated mirror. The monochromatization is ensured using the channel-cut Si(111) QuickExafs monochromator [23] and the harmonic rejection was done thanks to the B4C-coated second and third mirrors tilted at 4 mrad. The beam size was 1.50 mm x 0.45 mm (Horizontal x Vertical). The spectra were collected with an oscillating frequency of 2Hz at V K-edges in transmission utilizing gas ionization chambers as detectors. Three detectors in series allowed to measure during all the experiments a Vanadium

metal foil which could be used as reference to calibrate the incident energy beam. Several scans (in average 690 scans per spectrum) were recorded in order to ensure the reproducibility and to increase the signal-to-noise ratio. The ex situ samples were prepared by mixing uniformly the active material with cellulose, then pressed into pellets of 13 mm in diameter. Their spectra were recorded during 13 mins. In order to perform operando measurements, the electroactive material was homogeneously mixed with carbon black and polytetrafluoroethylene (PTFE) in the ratio of 30 : 60 : 10 (by wt.%) then pressed in a 13 mm pellet die under 10 tons to form films of ~300 μm in thickness. Half-cells were then assembled as operando cells using two Beryllium foils as X-ray transparent current collectors [24]. To avoid the strong absorption which might occur due to the high X-ray absorption coefficient of sodium, a tiny hole was made at the negative electrode, using a beam size of 1.50 mm x 0.45 mm (H x V).. Thanks to an automatic sample changer, three operando cells were measured in parallel with acquisition times of 6 mins spent successively on each sample. The main absorption edge observed at around 5485 eV on vanadium K edge XANES spectra is due to the $1s \rightarrow 4p$ dipole-allowed transition where the position of the edge can be related to the oxidation state of vanadium in the structure. The forbidden $1s \rightarrow 3d$ quadrupolar transitions may become allowed thanks to $3d$ - p orbital hybridization and lead to contributions in the pre-edge region. Their position and intensity are linked to the electronic structure and local environment (coordination number and the nature of the surrounding ligands) of vanadium [25–29]. The more distorted the vanadium site, the more intense is the pre-edge signal, versus that observed for highly symmetric $\text{V}(\text{O},\text{F})_6$ environment.

The electrochemical properties of the materials were tested in CR2032-type coin cells. The positive electrodes were prepared by the slurry tape casting method. A slurry containing 80 wt.% active material, 10 wt.% Carbon black, and 10 wt.% polyvinylidene fluoride (PVDF) dispersed in N-methyl-2-pyrrolidone (NMP) was casted on an Al foil, with a thickness of 150 μm , then dried overnight at 80 $^{\circ}\text{C}$ under vacuum. The mass loading of the as-prepared electrodes was around 2.5 $\text{mg}\cdot\text{cm}^{-2}$. A homemade electrolyte containing 1M solution of NaPF_6 (Strem Chemical; 99%) in ethylene carbonate and dimethyl carbonate (EC: DMC = 1: 1) with 2 wt.% of fluoroethylene carbonate (FEC) was used in all the electrochemical tests. The assembled cells were cycled in galvanostatic mode, at a C/10 cycling rate between 2.5 and 5.0 V vs. Na^+/Na . The rate C/10 corresponds to the exchange of 1 Na^+ in 10 hours.

2. Results and discussions

2.1. The complexity of the synthesis reaction

As already highlighted by Bianchini *et al.* [15] great discrepancies are reported in the literature for the unit cell parameters of $\text{Na}_3\text{V}_2(\text{PO}_4)_2\text{F}_3$. This is not surprising as only a strict control of the synthesis atmosphere (with no traces of oxygen) allows to obtain the stoichiometric phase. Most of the phases claimed in literature to be $\text{Na}_3\text{V}_2(\text{PO}_4)_2\text{F}_3$ are in fact likely to be characterized by a partial oxygen substitution for fluorine and thus, as a result of charge compensation, by the presence of V^{4+} according to the formula $\text{Na}_3\text{V}_2(\text{PO}_4)_2\text{F}_{3-y}\text{O}_y$ ($0 < y \leq 2$) [14]. As proposed earlier by our group [14], $\text{Na}_3\text{V}_2(\text{PO}_4)_2\text{F}_{3-y}\text{O}_y$ materials would hence be obtained according to the following reaction (1) with significant amounts of O_2 and CO_2 released:

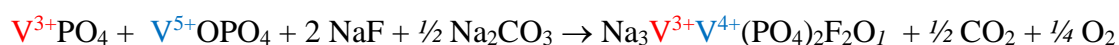
Equation (1)



We noted that the color of the powders varied gradually from dark grey ($y = 0$) to light green ($y = 0.5$) as the average oxidation state of vanadium was expected to evolve linearly from +3 (for $y = 0$) to +3.25 (for $y = 0.5$). No significant mass loss was recorded during the washing of the powders and a linear evolution of the unit cell parameters had been observed for $0 \leq y \leq 0.5$ [14]. In order to explore more in details the solid solution $\text{Na}_3\text{V}_2(\text{PO}_4)_2\text{F}_{3-y}\text{O}_y$ with $y > 0.5$, we synthesized in this study several compositions with $y = 0.75, 1.0, 1.5, 1.75$ and 2.0 according to equation (1). Surprisingly, the unit cell parameters evolve linearly only in the range of $0 \leq y \leq 1$. For $y > 1$, the unit cell parameters remain similar and very close to those reported for $\text{Na}_3(\text{VO})_2(\text{PO}_4)_2\text{F}$ by Tsirlin *et al.* (see **Figure S1** in supplementary information) [30]. Furthermore, we observe a significant mass loss for all the samples with $y > 1$ after being washed in water (up to 50 wt.% for $y = 2$). Interestingly, the as-prepared powders ($y > 1$) are dark green. However, after washing, a color change to bluish green is observed for all the powders. The solution recovered after washing is deep yellow. The comparison of the XAS spectra gathered in **Figure S2** confirms that the oxidation state of vanadium in all the materials obtained for $y > 1$ is +4. These results reveal that equation (1) does not correctly describe the synthesis of $\text{Na}_3\text{V}_2(\text{PO}_4)_2\text{F}_{3-y}\text{O}_y$.

In order to get more insight into the reaction involved in the synthesis of $\text{Na}_3\text{V}_2(\text{PO}_4)_2\text{F}_{3-y}\text{O}_y$, thermogravimetric analyses coupled to mass spectroscopy (TGA-MS) were

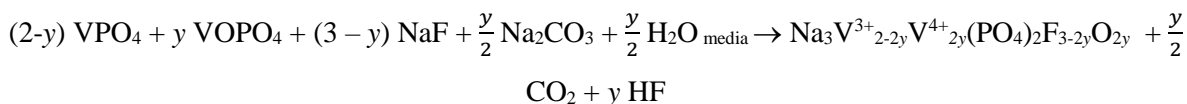
performed: first on the mixture of (2VPO₄ + 3NaF) as a reference and then on the mixture (VPO₄ + VOPO₄ + 2 NaF + ½ Na₂CO₃). The precursors were mixed using ball-milling, and then heated up to 650 °C for the former mixture and to 500 °C for the latter, at 5 °C.min⁻¹ under a continuous Ar flow. For the mixture of (2VPO₄ + 3NaF), no release of gas was detected before the tiny loss of fluorine (m/z = 19) from 450 °C (Erreur ! Source du renvoi introuvable.) that leads to the formation of Na₃V₂(PO₄)₂F_{3-δ}O₈ (δ ~ 0) with a small amount of oxygen defects. Note that despite several attempts, it was not possible to prevent the presence of oxygen traces during the thermal treatment and thus the formation of defects. Here the fluorine loss corresponds to ~ 0.5 % of the total mass and the δ value is thus expected to be infinitesimally small (**Figure S3**). According to equation (1), CO₂ and O₂ should always be released together during the reaction process. From the results obtained for the mixture (VPO₄ + VOPO₄ + 2 NaF + ½ Na₂CO₃), we can conclude that only CO₂ was detected, and not O₂ (**Figure 1**). This result, combined with the observations made during the synthesis (similar crystalline phase obtained whatever y for y > 1, with an increasing mass loss during washing with increasing y value) revealed that equation (1) proposed earlier by our group is actually not the proper description of the ongoing reaction. Indeed, applying equation (1) for y = 1 should have yielded:



into which all the V³⁺ ions from VPO₄ were maintained in their initial oxidation state whereas the only V⁵⁺ species from VOPO₄ were reduced to V⁴⁺ through the evolution of O₂, to finally obtain Na₃V³⁺V⁴⁺(PO₄)₂F₂O. Here in this work, we clearly confirm that no O₂ evolution is observed and that only V⁴⁺ is detected in the final product. Therefore, the actual electron exchange occurring during the synthesis reaction thus implies that V³⁺ → V⁴⁺ + 1 e⁻ (for V³⁺ from VPO₄) and V⁵⁺ + 1 e⁻ → V⁴⁺ (for V⁵⁺ from VOPO₄), so that the chemical reaction can be re-written for y = 1 as:

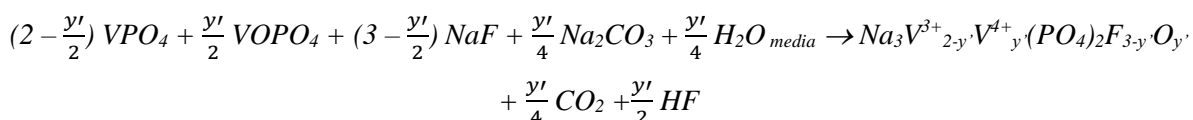


The formation of reactive COF₂ gas is in fact not detected. To explain this discrepancy, our hypothesis was at first to consider the high hygroscopic character of COF₂ which would promptly react with any trace of H₂O to form HF and CO₂. Nevertheless, as these two gases are not detected at the same time (CO₂ is detected first, and only then HF), we propose that Na₂CO₃ is decomposed first and releases CO/CO₂ and then, at higher temperatures, that fluorine is released and reacts with traces of water to form HF. The general equation (1) can be then re-written with y such as 0 ≤ y ≤ 1 and not 0 ≤ y ≤ 2:



In order to avoid possible confusion with our previous work, we choose to replace $2y$ by y' throughout this publication:

Equation (2)



(With $0 \leq y' \leq 2$ and $y' = 2y$)

As a conclusion, the general compositions of all the samples synthesized by Broux *et al.* are in fact $\text{Na}_3\text{V}^{3+}_{2-y'}\text{V}^{4+}_{y'}(\text{PO}_4)_2\text{F}_{3-y'}\text{O}_{y'}$ with $0 \leq y' \leq 1$ and not as proposed previously $\text{Na}_3\text{V}^{3+}_{2-y}\text{V}^{4+}_y(\text{PO}_4)_2\text{F}_{3-y}\text{O}_y$ ($0 \leq y \leq 0.5$) [14].

2.2. The stability of $\text{Na}_3\text{V}^{3+}_{2-y'}\text{V}^{4+}_{y'}(\text{PO}_4)_2\text{F}_{3-y'}\text{O}_{y'}$ materials in water

As just mentioned, all the as-prepared $\text{Na}_3\text{V}^{3+}_{2-y'}\text{V}^{4+}_{y'}(\text{PO}_4)_2\text{F}_{3-y'}\text{O}_{y'}$ powders were recovered after being washed in water to eliminate impurities such as $\text{Na}(\text{PO}_3)_3$ and $\text{Na}_2\text{V}_2\text{O}_5$. One might question if the phases are fully stable in water, or if water insertion, partial fluorine/hydroxyl exchange or even vanadium oxidation might be observed. The effect of washing the samples $\text{Na}_3\text{V}^{3+}_{2-y'}\text{V}^{4+}_{y'}(\text{PO}_4)_2\text{F}_{3-y'}\text{O}_{y'}$ ($0 \leq y' \leq 2$) with H_2O will be illustrated through the example of $\text{Na}_3(\text{VO})_2(\text{PO}_4)_2\text{F}$ ($y' = 2$), but the results obtained are representative of the series of compounds. The XRD pattern of the as-prepared $\text{Na}_3(\text{VO})_2(\text{PO}_4)_2\text{F}$ ($y' = 2$) reveals the presence of the main phase, of minor amounts of $\text{Na}(\text{PO}_3)_3$ and $\text{Na}_2\text{V}_2\text{O}_5$ and of tiny additional diffraction lines (Erreur ! Source du renvoi introuvable.a). The diffraction peaks corresponding to the impurities fully disappeared after washing as they are soluble in water and, as expected, the mass loss between the samples before and after washing was found to be less than 2 wt.%. Furthermore, the comparison of the cell parameters determined for $\text{Na}_3(\text{VO})_2(\text{PO}_4)_2\text{F}$ before and after washing reveals no changes and thus supports its stability in water (see **Table S1** in supporting information). Additionally, ICP-OES analyses confirm that the stoichiometry in Na, V and P is maintained to 3: 2: 2 upon washing and $\text{Na}_3(\text{VO})_2(\text{PO}_4)_2\text{F}$

is characterized by agglomerates of particles being less than 1 μm in diameter (**Figure S4**), with no apparent extra phases (impurities) at the particles' surface and in the grain boundaries.

The ^{31}P ss-NMR spectra recorded for $\text{Na}_3(\text{VO})_2(\text{PO}_4)_2\text{F}$ are identical before and after washing in water (Erreur ! Source du renvoi introuvable.**b**), showing that there is no change in the phosphorus local environment. The diamagnetic signals centered at ~ 0 ppm correspond to the $\text{P}(\text{OV}^{4+})_4$ local environment in the structure [14] and the splitting of the signals into two different peaks is due to the presence of two inequivalent local environments for phosphorus in $\text{Na}_3(\text{VO})_2(\text{PO}_4)_2\text{F}$ structure. ^{23}Na ss-NMR was also recorded for the washed and unwashed powders in order to get insight into the stability of the phases. The spectra are compared for $\text{Na}_3(\text{VO})_2(\text{PO}_4)_2\text{F}$ in **Figure S5** in the supporting information. They exhibit two main resonances at 76 ppm and 120 ppm corresponding to Na nuclei interacting with two neighboring V^{4+} ions, and with a combination of one V^{3+} and one V^{4+} , respectively. These observations show: (i) that there are traces of V^{3+} present in both powders and (ii) the high stability in water as no major changes of the main resonances are observed.

Similar observations were made by IR spectroscopy (**Figure 2c**). The characteristic stretching modes of $\text{V}=\text{O}$, and $\text{P}-\text{O}$ (in PO_4^{3-}) bonds were identified in the as-prepared material and remained unchanged after washing. In addition, no signature revealing the presence of structural (inserted) H_2O molecules and of hydroxyl groups due to an exchange with fluorine was detected in the washed sample: they would have been expected as a large band between 2300 and 3500 cm^{-1} and as a narrow band at 3300 cm^{-1} respectively [31]. The tiny signal recorded in the region of 3000 - 4000 cm^{-1} was attributed to the presence of traces of water adsorbed at the particles' surface. The vibrations observed in the region of 500 - 700 cm^{-1} can be attributed to the stretching mode of $\text{V}-\text{O}/\text{V}-\text{F}$ bonds or to the deformation mode of PO_4 groups in the structure.

Combining all these findings on the whole range of $0 \leq y' \leq 2$ compositions, we can conclude that the series of compounds $\text{Na}_3\text{V}^{3+}_{2-y'}\text{V}^{4+}_{y'}(\text{PO}_4)_2\text{F}_{3-y'}\text{O}_{y'}$ is stable in water. The washing performed as a final step at the end of the synthesis to remove possible (soluble) impurities is thus not detrimental to the composition and structural integrity of the materials, and as it will be discussed later, to their electrochemical performance. The stability of these phases in aqueous media is a key factor that makes them attractive positive electrode materials for Na-ion batteries as: (i) they can be stored in air for long time without any degradation of their electrochemical performance, (ii) they can

be processed in water to develop aqueous electrode formulation and (iii) they can be used as positive electrodes in aqueous rechargeable Na-ion batteries, as recently proposed by Kumar *et al.*[32]

2.3. The crystal structure of $\text{Na}_3\text{V}^{3+}_{2-y'}\text{V}^{4+}_{y'}(\text{PO}_4)_2\text{F}_{3-y'}\text{O}_{y'}$ ($0 \leq y' \leq 2$)

Bianchini *et al.* have shown for the first time that the structure of the stoichiometric $\text{Na}_3\text{V}_2(\text{PO}_4)_2\text{F}_3$ phase (i.e. the pure V^{3+} composition) should be described in an orthorhombic unit cell (*Amam*) due to a specific distribution of the Na^+ ions over three different crystallographic sites within the tunnels of this polyanionic framework, that allows a decrease of the electrostatic interactions between the Na^+ ions [15]. Later, Broux *et al.* have shown that the orthorhombic distortion was maintained for partial oxygen substitution for fluorine, despite being less obvious to identify from a simple observation of the synchrotron X-ray diffraction pattern for $0.5 < y' \leq 1$ [14]. Indeed, the clear orthorhombic splitting at the (400) and (040) diffraction lines was no longer observed (see Figure 2 in [14]). Nevertheless, the orthorhombic distortion was maintained and required, as it was leading to the best calculation of the experimental pattern and to the good description of the structure with regular PO_4 groups as well as to the minimization of the interactions between the Na^+ ions [14]. In the frame of this study, it was thus essential to revisit the structure of $\text{Na}_3\text{V}^{3+}_{2-y'}\text{V}^{4+}_{y'}(\text{PO}_4)_2\text{F}_{3-y'}\text{O}_{y'}$ with y' such as $1 < y' \leq 2$, i.e. for the oxygen-rich compositions. Indeed, up to now, by analogy with the tetragonal structure (*P4₂/mnm*) proposed by Le Meins *et al.* for the phase reported to be $\text{Na}_3\text{V}_2(\text{PO}_4)_2\text{F}_3$ [33], all the compositions (whatever the value of y') were described in *P4₂/mnm* and not in *Amam*.

The structures of $\text{Na}_3\text{V}_2(\text{PO}_4)_2\text{F}_{1.5}\text{O}_{1.5}$ ($y'=1.5$) and $\text{Na}_3(\text{VO})_2(\text{PO}_4)_2\text{F}$ ($y'=2.0$) were analyzed in both *Amam* and *P4₂/mnm* S.G. As shown in **Figures S6** and **S7** and in good agreement with the observation made already for $\text{Na}_3\text{V}_2(\text{PO}_4)_2\text{F}_2\text{O}$ ($y' = 1.0$) [14] no peak splitting of the (400) and (040) diffraction lines were observed. The indexation of the diffraction lines can thus be made considering a tetragonal unit cell described in the space group *P4₂/mnm* with identical a and b cell parameters. The evolution of the cell parameters is given in **Figure 3**, in comparison with those reported by Park *et al.* [7], by Serras *et al.*[34] for oxygen-rich composition and by Tsirlin *et al.* [30] for the end member $\text{Na}_3(\text{VO})_2(\text{PO}_4)_2\text{F}$. Note that all these results are consistent and in very good agreement. Indeed, as shown in **Table 1**, a linear decrease of a , b and c is observed with an increasing substitution of oxygen for fluorine: this

latter is compensated by the oxidation of V^{3+} into V^{4+} and by the shrinking of the $VO_4(F,O)_2$ octahedra with the formation of more covalent V-O bonds in the square planes and of vanadyl-type bonds along the axis of the bi-octahedral units $V_2O_8(F,O)_3$. It shows the rather good miscibility between oxygen engaged into a vanadyl-type bond and fluorine, and thus allowing the formation of a solid solution between the two end members $Na_3V^{3+}_2(PO_4)_2F_3$ and $Na_3(V^{4+}O)_2(PO_4)_2F$. Nevertheless, in order to discriminate between the two structural hypotheses (the orthorhombic unit cell versus the tetragonal one) for $Na_3V_2(PO_4)_2F_{1.5}O_{1.5}$ and $Na_3(VO)_2(PO_4)_2F$, an in-depth analysis of the Fourier difference maps, of the bonds calculated for the PO_4 and $VO_4(F,O)_2$ polyhedra and of the Na^+ - Na^+ distances, is required.

All the details of these analyses are given in supplementary information: in **Figure S6** and **Table S2** for $Na_3V_2(PO_4)_2F_{1.5}O_{1.5}$, and in **Figure S7** and **Table S3** for $Na_3(VO)_2(PO_4)_2F$. These results do not allow to choose easily between the two models. Nevertheless, they suggest that the *Amam* description is the most appropriate. Indeed, a slightly better minimization of the Fourier difference maps is obtained, the XRD patterns are calculated with a smaller number of diffraction lines (in $P4_2/mnm$, many are calculated with null intensities), and longer Na^+ - Na^+ distances are obtained allowing a minimization of the electrostatic repulsions within the diffusion channels. Nevertheless, for the specific case of $Na_3(VO)_2(PO_4)_2F$, as highlighted by the enlargements given in **Figure 4**, some low intensity diffraction peaks are not indexed in the orthorhombic cell. The doubling of the three unit cell parameters ($2 a \times 2 b \times 2 c$) is required to index all the reflections, and in that case the smaller unit cell required to describe the structure is monoclinic ($P2_1/m$) with a vector of modulation $q = \frac{1}{2} b^* + \frac{1}{2} c^*$ (**Figure 4**, bottom) associated to the ordering of the Na^+ ions along the b and c axes. The distribution of the Na^+ ions within the diffusion channels and the modulation waves associated to each Na^+ site are given in supplementary information in **Figure S8** and **Table S4**. Note that the thermal displacement parameters (*Biso*) associated to the different atoms (Na, V, P and O/F) are homogeneous from one site to another for a given atom, and in good agreement with the values expected: 1, 0.11, 0.08 and 0.10 respectively. The single PO_4^{3-} anionic group present in the structure is such that the P-O bonds vary between 1.48 and 1.59 Å, whereas two vanadium sites are observed, one with a short V=O vanadyl type bond of 1.53 Å and the other one with a longer V=O vanadyl type bond at 1.71 Å. Electron diffraction experiments were performed to try to confirm the monoclinic unit cell and the presence of the vector of modulation. Unfortunately, the sample is unstable and decomposed under the electron beam, at ambient and low temperatures.

IR spectroscopy has been used in order to get a better insight into the formation of the V=O vanadyl-type bonds and their spreading within the framework of $\text{Na}_3\text{V}^{3+}_{2-y'}\text{V}^{4+}_{y'}(\text{PO}_4)_2\text{F}_{3-y'}\text{O}_{y'}$ with y' such as $0 \leq y' \leq 2$. The comparison of the overall spectra is given in **Figure S9** in the wavenumber range of 400 - 3000 cm^{-1} , and the corresponding enlargements in **Figure 2d** in the wavenumber range of 800 - 1300 cm^{-1} . The tiny stretching mode observed at $\sim 940 \text{ cm}^{-1}$ for $\text{Na}_3\text{V}_2(\text{PO}_4)_2\text{F}_3$ corresponds to the localized V=O vanadyl type defects present in a fluorine-rich composition [35,36]. Two vibrational bands are observed at $\sim 910 \text{ cm}^{-1}$ and $\sim 940 \text{ cm}^{-1}$ when oxygen is partially substituted for fluorine in $\text{Na}_3\text{V}^{3+}_{2-y'}\text{V}^{4+}_{y'}(\text{PO}_4)_2\text{F}_{3-y'}\text{O}_{y'}$, their overtone bands being at $\sim 1840 \text{ cm}^{-1}$ and $\sim 1870 \text{ cm}^{-1}$. The intensity of the signal at $\sim 910 \text{ cm}^{-1}$ increases while the one at $\sim 940 \text{ cm}^{-1}$ decreases when the y' value moving from 0 to 2, and the vibration at $\sim 940 \text{ cm}^{-1}$ is very similar to the vanadyl stretching mode observed for $\text{Na}_3\text{V}_2(\text{PO}_4)_2\text{F}_3$. The presence of these two signals indicates two different local environments for the vanadyl bond V=O: the one at 940 cm^{-1} would correspond to vanadyl bonds with V-F bond opposite along the axis of the bi-octahedral unit, and that at 910 cm^{-1} to vanadyl bonds with V=O bond opposite along the axis of the bi-octahedral unit.

The comparison of the structures of $\text{Na}_3\text{V}_2(\text{PO}_4)_2\text{F}_{1.5}\text{O}_{1.5}$ and $\text{Na}_3(\text{VO})_2(\text{PO}_4)_2\text{F}$ with those we previously reported for $\text{Na}_3\text{V}^{3+}_{2-y'}\text{V}^{4+}_{y'}(\text{PO}_4)_2\text{F}_{3-y'}\text{O}_{y'}$ ($0 \leq y' \leq 1$) shows that the orthorhombic structural model is the most appropriate to describe the overall solid solution $\text{Na}_3\text{V}_2(\text{PO}_4)_2\text{F}_3 - \text{Na}_3(\text{VO})_2(\text{PO}_4)_2\text{F}$, with a modulated structure required to describe the distribution of the Na^+ ions in the vanadyl-rich composition $\text{Na}_3(\text{VO})_2(\text{PO}_4)_2\text{F}$.

2.4. Electrochemical properties

The electrochemical properties of $\text{Na}_3\text{V}_2(\text{PO}_4)_2\text{F}_2\text{O}$, $\text{Na}_3\text{V}_2(\text{PO}_4)_2\text{F}_{1.5}\text{O}_{1.5}$ and $\text{Na}_3(\text{VO})_2(\text{PO}_4)_2\text{F}$ as the positive electrodes in half cells vs. Na are compared in **Figure 5** to those of our reference [9], optimized carbon-coated $\text{Na}_3\text{V}_2(\text{PO}_4)_2\text{F}_3$. The electrochemical profiles were obtained at a cycling rate of C/10 per Na^+ in the potential range 2.5 - 4.3 V vs. Na^+/Na . As expected larger polarizations are observed for the oxygen substituted compositions as the materials were not carbon coated. Nevertheless, for all the compositions, about two Na^+ ions can be extracted reversibly in two voltage domains in this potential window: the first Na^+ ion at 3.6 – 3.7 V vs Na^+/Na and the second Na^+ ion at 4.0 – 4.20 V vs Na^+/Na . For the two end members $\text{Na}_3\text{V}_2(\text{PO}_4)_2\text{F}_3$ ($y' = 0$) and $\text{Na}_3(\text{VO})_2(\text{PO}_4)_2\text{F}$ ($y' = 2$), voltage-composition “plateaus” can be observed that imply the formation of several intermediate phases during

charge/discharge, whose crystal structures were reported by Bianchini *et al.*[37] and Sharma *et al.* [38], respectively. For the compositions corresponding to partial oxygen substitution for fluorine in $\text{Na}_3\text{V}^{3+}_{2-y'}\text{V}^{4+}_{y'}(\text{PO}_4)_2\text{F}_{3-y'}\text{O}_{y'}$, the voltage-composition signatures are sloping indicating solid solution type mechanisms, with a continuous Na^+ de-intercalation and re-intercalation from/in the structure during charge/discharge. In these systems, phase transitions - when observed - are associated to charge and/or alkali orderings. In fact, no superstructure was observed in the pristine materials $\text{Na}_3\text{V}^{3+}_{2-y'}\text{V}^{4+}_{y'}(\text{PO}_4)_2\text{F}_{3-y'}\text{O}_{y'}$ ($y' \neq 0, y' \neq 2$) showing that V^{3+} and V^{4+} (as well as the terminal O and F anions in the bi-octahedral units) are not long-range ordered within the framework. On the contrary, for the V^{3+} only composition $\text{Na}_3\text{V}_2(\text{PO}_4)_2\text{F}_3$ and for the V^{4+} only composition $\text{Na}_3(\text{VO})_2(\text{PO}_4)_2\text{F}$, charge and alkali orderings can be stabilized, and are indeed observed, as they allow to minimize (i) the strains within the host structure (with the homogeneous distribution of the bond lengths) and (ii) the electrostatic repulsions between the alkali ions within the diffusion channels. It is also interesting to highlight that the average voltage corresponding to Na^+ extraction decreases continuously upon oxygen substitution for fluorine. This decrease is induced by the formation of strongly covalent vanadyl-type bonds that induce a so-called “reverse inductive effect” and promote the activation of the $\{\text{V}^{5+}=\text{O}\}^{3+}/\{\text{V}^{4+}=\text{O}\}^{2+}$ redox couple at lower voltage.

Theoretically more than 2 Na^+ ions can be electrochemically extracted per formula unit of $\text{Na}_3\text{V}^{3+}_{2-y'}\text{V}^{4+}_{y'}(\text{PO}_4)_2\text{F}_{3-y'}\text{O}_{y'}$, up to 3 Na^+ ions for $\text{Na}_3\text{V}_2(\text{PO}_4)_2\text{F}_3$ with an oxidation of V^{3+} to an average oxidation state of $\text{V}^{4.5+}$. The reversible de-intercalation and re-intercalation of 3 Na^+ ions would lead to an increase of the capacity delivered by $\text{Na}_3\text{V}_2(\text{PO}_4)_2\text{F}_3$ of 50%. Very recently, a third plateau that would correspond to the extraction of an extra 0.5 Na^+ was observed at 4.75 V vs Na^+/Na for $\text{Na}_3\text{V}_2(\text{PO}_4)_2\text{F}_3$ [39]. This overall extraction of 2.5 Na^+ ions during the first charge apparently leads to an irreversible transformation of the structure with the formation of a so-called new modification of $\text{Na}_3\text{V}_2(\text{PO}_4)_2\text{F}_3$ described in a disordered tetragonal structure ($I4/mmm$) that allows for the re-insertion of only 1.5 Na^+ in the potential window of interest for applications. It was hence interesting to consider the behavior of oxygen substituted $\text{Na}_3\text{V}^{3+}_{2-y'}\text{V}^{4+}_{y'}(\text{PO}_4)_2\text{F}_{3-y'}\text{O}_{y'}$ at high voltages.

Figure 6 gives the comparison of $\text{Na}_3\text{V}_2(\text{PO}_4)_2\text{F}_3$ and $\text{Na}_3\text{V}_2(\text{PO}_4)_2\text{F}_{1.5}\text{O}_{1.5}$ when used as positive electrodes electrochemically cycled up to 5 V vs. Na^+/Na . Theoretically 3 Na^+ ions can be de-intercalated from $\text{Na}_3\text{V}_2(\text{PO}_4)_2\text{F}_3$ with the oxidation of vanadium up to an average oxidation state of +4.5 thus being an ion-limited reaction. In the case of $\text{Na}_3\text{V}_2(\text{PO}_4)_2\text{F}_{1.5}\text{O}_{1.5}$, 2.5 Na^+ ions should be extracted with the oxidation of vanadium up to the average oxidation

state of 5+ and thus a redox-limited reaction. The data plotted in **Figure 6** reveal that in continuous galvanostatic cycling conditions at C/10 per Na⁺ ion, a third plateau is observed during the first charge of Na // Na₃V₂(PO₄)₂F₃ at high voltage. It corresponds to a voltage jump of 0.5 V after the de-intercalation of 2 Na⁺ ions from the structure and to an additional exchange of 0.5 extra electrons, in good agreement with the results already reported by Yan *et al.* [39]. The derivative curves of the first and second cycles given in **Figure 6b** confirm the irreversible transformation occurring along the third plateau, with sharp peaks associated to successive biphasic reactions during the first charge and then, during the next discharge and cycles, broader peaks showing a drastic change in the reaction mechanism. The inset in **Figure 6a** compares the evolution of the charge and discharge capacity upon cycling and highlights that the overcapacity is only observed during the first charge at high voltage and is never recovered then in the potential window practically required for a Na-ion battery developed for the applications. For Na//Na₃V₂(PO₄)₂F_{1.5}O_{1.5} a voltage jump of ~ 0.5 V is observed at high voltage, as for Na₃V₂(PO₄)₂F₃, after the de-intercalation of 2 Na⁺ ions from the structure of Na₃V₂(PO₄)₂F_{1.5}O_{1.5}. No third plateau is observed but rather a continuous voltage increase when the upper voltage limit is increased to 5 V vs Na⁺/Na until the full Na⁺ de-intercalation from Na_xV₂(PO₄)₂F_{1.5}O_{1.5} (Erreur ! Source du renvoi introuvable.c). The value of $x = 0$ found is intriguing and unexpected, as the number of transition metal redox centers is such that only the exchange of 2.5 Na⁺ would be possible. This extra capacity at high voltage region for Na//Na₃V₂(PO₄)₂F_{1.5}O_{1.5} would thus be associated with the degradation of the electrolyte. This hypothesis is further supported by the fact that, on the contrary to the observation made for Na₃V₂(PO₄)₂F₃, the first charge to high voltage does not induce any modification of the next cycles, as also highlighted by the derivative curves given in **Figure 6d**.

In order to get more insight into the redox processes involved during these first charges to high voltage, *operando* X-ray absorption spectroscopy (XAS) spectra at the Vanadium K edge were measured upon cycling. The electrochemical data recorded in the *in situ* electrochemical cells are given in **Figure 7a** and **Figure 7c** for Na//Na₃V₂(PO₄)₂F₃ and Na//Na₃V₂(PO₄)₂F_{1.5}O_{1.5} respectively. Broux *et al.* have shown, especially by the analysis of the pre-edge of the XAS spectra, that the de-intercalation of the first Na⁺ ion from Na₃V₂(PO₄)₂F₃ is associated to the formation of V³⁺-V⁴⁺ pairs in the bi-octahedral units. The subsequent de-intercalation of the second Na⁺ ion leads to the formation of disproportionate V³⁺-V⁵⁺ pairs [28]. Indeed, significant modifications were observed during the oxidation of V³⁺ into V⁴⁺ and V⁵⁺ with a global shift to higher energy for the pre-edge and for the edge upon

oxidation. The presence of V^{5+} in $Na_1V_2(PO_4)_2F_3$ at 4.3 V vs Na^+/Na was supported by the observation of a characteristic intense peak signal at 5471 eV [28]. Similar results were obtained in the present study, as shown in [Erreur ! Source du renvoi introuvable.](#)**b**, and as highlighted by the changes observed between the spectra #1, #20 and #40. Surprisingly, upon further Na^+ de-intercalation, no shift of the absorption edge is observed between the spectrum #40 corresponding to $Na_1V_2(PO_4)_2F_3$ and the spectrum #57 recorded at the end of the charge and corresponding to a theoretical composition of $Na_{\sim 0.15}V_2(PO_4)_2F_3$ (**Figure 8a**, and **Figure S10** that gives the evolution in the energy of the absorption edge). This result suggests that vanadium does not participate at all into the redox processes in this potential domain (on the third plateau). Indeed, a careful inspection of the XANES results show that only the pre-edge is modified with an increase of the intensity versus that observed for the spectrum #40: this suggests that the local environment around vanadium is increasingly distorted, and thus that significant modification of the vanadium environment is observed, but not of the vanadium oxidation state. Note that similar results are observed in [39] in Figure 7b-c, even if interpreted differently, with a great similarity between the spectra recorded at the Vanadium L-edge and Oxygen K edge on the compositions assumed to be $Na_1V_2(PO_4)_2F_3$ and $Na_{0.25}V_2(PO_4)_2F_3$. These results suggest a drastic reorganization and instability of the structure of $Na_1V_2(PO_4)_2F_3$ when the battery is overcharged. The XRD and NMR results reported in [39] suggest in fact a strong degradation of the long range atomic structure. At this stage of our understanding, we suggest that the electrons exchanged at high voltage would be associated to the oxidation of the electrolyte, occurring in parallel to the structure degradation. This highly charged state has to be revisited considering this hypothesis, and considering especially the Na/V ratio.

Interestingly, the XAS spectrum of $Na_3V_2(PO_4)_2F_{1.5}O_{1.5}$ is significantly different from that of $Na_3V_2(PO_4)_2F_3$, with an additional intense signal at 5469.5 eV in the pre-edge region (**Figure 7d** vs **Figure 7b**). Indeed, in this mixed valence composition, the stoichiometry is such that one V^{3+} exists besides three V^{4+} , those being engaged in vanadyl-type bonds $\{V^{4+}=O\}^{2+}$. The environments of V^{3+} are ‘quasi’-symmetric $VO_4(F,O)_2$ sites with six $V^{3+}-(F,O)$ bond lengths around 1.9 - 2.0 Å, whereas those of V^{4+} are highly distorted $VO_4O(F,O)$ site with a long $V^{4+}-(F,O)$ bond around 2.2 Å and a short and highly covalent $V^{4+}=O$ bond around 1.6 Å [15,29,30]. These latter vanadyl-type environments are in fact responsible for the intense signal at 5469.5 eV. Upon charge, this signal decreases gradually in intensity while a new signal grows at 5471.5 eV ([Erreur ! Source du renvoi introuvable.](#), spectra #1 to #71). At the same time, a continuous shift of the absorption edge is also observed from 5481.9 eV for the spectrum #1 to

5484.6 eV for the spectrum #70. These evolutions confirm the oxidation of vanadium in the voltage range 3.56 – 4.12 V vs Na⁺/Na. Nevertheless, all the spectra recorded at higher voltage remain identical (see **Figure 8b** that compares the spectrum #71 and the final spectrum #83), showing also that the overcapacity observed is not associated with the participation of vanadium to the redox processes, but most probably also to electrolyte decomposition. In that case, on the contrary to the observations made for Na₃V₂(PO₄)₂F₃ no modification of the pre-edge is observed, suggesting that the local structure around vanadium remains the same.

It is interesting to highlight that the highly de-intercalated Na_xV₂(PO₄)₂F₃ has been predicted to be thermodynamically unstable by theoretical calculations [40,41]. In our opinion it has thus to be considered with careful attention, considering especially the results just discussed. Furthermore, as mentioned just before, partial oxygen substitution for fluorine could be seen as a stabilizing factor in the overcharge state of the battery. Indeed, the highly de-intercalated Na_xV₂(PO₄)₂F_{1.5}O_{1.5} appears stable, at least over a few cycles. Finally, it is also interesting to mention that, if it occurs or if it should occur, the overcapacity associated with the de-intercalation of extra Na⁺ ions (*vs.* the “classical” 2 Na⁺ ions) should be obtained at lower potential for Na₃V₂(PO₄)₂F_{1.5}O_{1.5}, as oxygen substitution for fluorine was shown to shift down the average voltage of the reaction. This shortening of the third plateau for Na₃V₂(PO₄)₂F_{1.5}O_{1.5} is perhaps another argument to question further the origin of the mechanism involved at high voltage.

3. Conclusions

The series of compounds Na₃V³⁺_{2-y'}V⁴⁺_{y'}(PO₄)₂F_{3-y'}O_{y'} (0 ≤ y' ≤ 2) were proven to be completely stable in water. Indeed, a washing in water can be used to remove soluble and undesirable impurities formed during the synthesis, without any detrimental impact on their electrochemical performance in batteries. It is thus possible to develop aqueous electrode formulations or even to use them at the positive electrode in aqueous batteries [32,42]. The orthorhombic structural model appears as the most appropriate to describe the overall solid solution Na₃V₂(PO₄)₂F₃ - Na₃(VO)₂(PO₄)₂F, with a modulated structure required to describe the distribution of the Na⁺ ions in the vanadyl-rich composition Na₃(VO)₂(PO₄)₂F. The minimization of the electrostatic repulsions within the diffusion channels throughout the framework appears as the main driving force for the stabilization of the structure. Extra capacity can be obtained for Na₃V₂(PO₄)₂F₃ and oxygen substituted Na₃V₂(PO₄)₂F_{3-y'}O_{y'} compositions

by increasing the upper cut-off voltage to 5.0 V vs. Na⁺/Na; however, this capacity is irreversible. Whatever the compositions, the vanadium redox center appears not to be involved beyond the deintercalation of 2 Na⁺ ions per formula unit. Nevertheless, for the fluorine-rich compositions, the overcharge leads to a drastic modification of the structure with the formation of a highly disordered structure: the local environment of the vanadium ions is modified, despite their oxidation state is not. On the contrary, the oxygen-rich compositions are stable during the overcharge as the local environment of vanadium nor its oxidation state are modified. In our opinion, it is thus essential to revisit: (i) the mechanisms involved at high voltage in Na₃V₂(PO₄)₂F₃ and (ii) the impact of a small oxygen substitution for fluorine as the presence of vanadyl type bonds seems to have a stabilizing effect on the structure at high voltage.

Author information

Corresponding author

* E-mail: laurence.croguennec@icmcb.cnrs.fr

Notes

The authors declare no competing financial interest

Acknowledgements

The authors thank the RS2E Network for the funding of LHBN's PhD thesis, the RS2E and Alistore-ERI networks for the funding of TB's postdoctoral fellowship, as well as the financial support of Région Nouvelle Aquitaine, of the French National Research Agency (STORE-EX Labex Project ANR-10-LABX-76-01 and SODIUM Descartes project ANR-13-DESC-0001-02) and of the European Union's Horizon 2020 research and innovation program under the Grant Agreement No. 646433-NAIADES. The authors also want to thank François WEILL (ICMCB) for electron diffraction experiments, Jacques DARRIET (ICMCB) for discussions of the modulated structures, as well as Cathy DENAGE, Laetitia ETIENNE and Eric LEBRAUD (ICMCB) for their help with SEM, ICP-OES and XRD analyses, respectively. This work was supported by a public grant overseen by the French National Research Agency (ANR) as part of the “*Investissements d’Avenir*” program (Reference: ANR-EQPX45).

References

- [1] J.B. Goodenough, Y. Kim, Challenges for Rechargeable Li Batteries, *Chem. Mater.* 22 (2010) 587–603.
- [2] J.-Y. Hwang, S.-T. Myung, Y.-K. Sun, Sodium-ion batteries: present and future, *Chem. Soc. Rev.* 46 (2017) 3529–3614.
- [3] C. Delmas, J.-J. Braconnier, C. Fouassier, P. Hagenmuller, Electrochemical intercalation of sodium in Na_xCO_2 bronzes, *Solid State Ionics.* 3–4 (1981) 165–169.
- [4] B.V.R. Reddy, R. Ravikumar, C. Nithya, S. Gopukumar, High performance Na_xCoO_2 as a cathode material for rechargeable sodium batteries, *J. Mater. Chem. A.* 3 (2015) 18059–18063.
- [5] J. Gopalakrishnan, K. Kasthuri Rangan, $\text{V}_2(\text{PO}_4)_3$: A Novel NASICON-Type Vanadium Phosphate Synthesized by Oxidative Deintercalation of Sodium from $\text{Na}_3\text{V}_2(\text{PO}_4)_3$, *Chem. Mater.* 4 (1992) 747–749.
- [6] F. Lalère, V. Seznec, M. Courty, R. David, J.N. Chotard, C. Masquelier, Improving the energy density of $\text{Na}_3\text{V}_2(\text{PO}_4)_3$ -based positive electrodes through V/Al substitution, *J. Mater. Chem. A.* 3 (2015) 16198–16205.
- [7] Y.U. Park, D.H. Seo, H. Kim, J. Kim, S. Lee, B. Kim, K. Kang, A family of high-performance cathode materials for Na-ion batteries, $\text{Na}_3(\text{VO}_{1-x}\text{PO}_4)_2\text{F}_{1+2x}$ ($0 \leq x \leq 1$): Combined first-principles and experimental study, *Adv. Funct. Mater.* 24 (2014) 4603–4614.
- [8] A. Ponrouch, R. Dedryvere, D. Monti, A.E. Demet, J.M. Ateba Mba, L. Croguennec, C. Masquelier, P. Johansson, M.R. Palacin, Towards high energy density sodium ion batteries through electrolyte optimization, *Energy Environ. Sci.* 6 (2013) 2361–2369.
- [9] T. Broux, F. Fauth, N. Hall, Y. Chatillon, M. Bianchini, T. Bamine, J. Leriche, E. Suard, D. Carlier, Y. Reynier, L. Simonin, C. Masquelier, L. Croguennec, High Rate Performance for Carbon-Coated $\text{Na}_3\text{V}_2(\text{PO}_4)_2\text{F}_3$ in Na-Ion Batteries, *Small Methods.* 2 (2018) 1800215.
- [10] W. Zhou, L. Xue, X. Lü, H. Gao, Y. Li, S. Xin, G. Fu, Z. Cui, Y. Zhu, J.B. Goodenough, $\text{Na}_x\text{MV}(\text{PO}_4)_3$ (M = Mn, Fe, Ni) Structure and Properties for Sodium Extraction, *Nano Lett.* 16 (2016) 7836–7841.
- [11] F. Chen, V.M. Kovrugin, R. David, O. Mentré, F. Fauth, J. Chotard, C. Masquelier, A NASICON-Type Positive Electrode for Na Batteries with High Energy Density: $\text{Na}_4\text{MnV}(\text{PO}_4)_3$, *Small Methods.* 1800218 (2018).
- [12] A.M. Abakumov, M. V. Zakharkin, O.A. Drozhzhin, E. V. Antipov, D. Chernyshov, I. V. Tereshchenko, K.J. Stevenson, Enhancing Na^+ Extraction Limit through High Voltage Activation of the NASICON-Type $\text{Na}_4\text{MnV}(\text{PO}_4)_3$ Cathode, *ACS Appl. Energy Mater.* 1 (2018) 5842–5846.
- [13] P. Serras, V. Palomares, A. Goñi, I. Gil De Muro, P. Kubiak, L. Lezama, T. Rojo, High voltage cathode materials for Na-ion batteries of general formula $\text{Na}_3\text{V}_2\text{O}_{2x}(\text{PO})_2\text{F}_{3-2x}$, *J. Mater. Chem.* 22 (2012) 22301–22308.
- [14] T. Broux, T. Bamine, F. Fauth, L. Simonelli, W. Olszewski, C. Marini, M. Ménétrier, D. Carlier, C. Masquelier, L. Croguennec, Strong Impact of the Oxygen Content in

- $\text{Na}_3\text{V}_2(\text{PO}_4)_2\text{F}_{3-y}$ Oy ($0 \leq y \leq 0.5$) on Its Structural and Electrochemical Properties, *Chem. Mater.* 28 (2016) 7683–7692.
- [15] M. Bianchini, N. Brisset, F. Fauth, F. Weill, E. Elkaim, E. Suard, C. Masquelier, L. Croguennec, $\text{Na}_3\text{V}_2(\text{PO}_4)_2\text{F}_3$ Revisited : A High-Resolution Diffraction Study, *Chem. Mater.* 26 (2014) 4238–4247.
- [16] C. Shen, H. Long, G. Wang, W. Lu, L. Shao, K. Xie, $\text{Na}_3\text{V}_2(\text{PO}_4)_2\text{F}_3$ @C dispersed within carbon nanotube frameworks as a high tap density cathode for high-performance sodium-ion batteries, *J. Mater. Chem. A* 6 (2018) 6007–6014.
- [17] C. Zhu, C. Wu, C. Chen, P. Kopold, P.A. van Aken, J. Maier, Y. Yu, A High Power–High Energy $\text{Na}_3\text{V}_2(\text{PO}_4)_2\text{F}_3$ Sodium Cathode: Investigation of Transport Parameters, Rational Design and Realization, *Chem. Mater.* 29 (2017) 5207–5215.
- [18] T. Jiang, G. Chen, A. Li, C. Wang, Y. Wei, Sol – gel preparation and electrochemical properties of $\text{Na}_3\text{V}_2(\text{PO}_4)_2\text{F}_3/\text{C}$ composite cathode material for lithium ion batteries, 478 (2009) 604–607.
- [19] N. Hall, S. Boulineau, S. Launois, L. Simonin, L. Croguennec, C. Masquelier, Method for preparing a $\text{Na}_3\text{V}_2(\text{PO}_4)_2\text{F}_3$ particulate material, French Patent 2016.
- [20] J. Rodríguez-Carvajal, Recent advances in magnetic structure determination by neutron powder diffraction, *Phys. B Condens. Matter* 192 (1993) 55–69.
- [21] V. Petříček, M. Dušek, L. Palatinus, Crystallographic Computing System JANA2006 : General features, *Z. Krist.* 229 (2014) 345–352.
- [22] K. Momma, F. Izumi, VESTA: A three-dimensional visualization system for electronic and structural analysis, *J. Appl. Crystallogr.* 41 (2008) 653–658.
- [23] E. Fonda, A. Rochet, M. Ribbens, L. Barthe, S. Belin, V. Briois, The SAMBA quick-EXAFS monochromator: XAS with edge jumping, *J. Synchrotron Radiat.* 19 (2012) 417–424.
- [24] J.B. Leriche, S. Hamelet, J. Shu, M. Morcrette, C. Masquelier, G. Ouvrard, M. Zerrouki, P. Soudan, S. Belin, E. Elkaim, F. Baudalet, An Electrochemical Cell for Operando Study of Lithium Batteries Using Synchrotron Radiation, *J. Electrochem. Soc.* 157 (2010) A606.
- [25] J. Wong, F.W. Lytle, R.P. Messmer, D.H. Maylotte, K-edge absorption spectra of selected vanadium compounds, *Phys. Rev. B - Condens. Matter Mater. Phys.* 30 (1984).
- [26] B. Poumellec, V. Kraizman, Y. Aifa, R. Cortès, A. Novakovich, R. Vedrinskii, Experimental and theoretical studies of dipole and quadrupole contributions to the vanadium, *Phys. Rev. B - Condens. Matter Mater. Phys.* 58 (1998) 6133–6146.
- [27] Z.Y. Wu, D.C. Xian, T.D. Hu, Y.N. Xie, Y. Tao, C.R. Natoli, E. Paris, A. Marcelli, Quadrupolar transitions and medium-range-order effects in metal K-edge X-ray absorption spectra of 3 d transition-metal compounds, *Phys. Rev. B - Condens. Matter Mater. Phys.* 70 (2004) 1–4.
- [28] T. Broux, T. Bamine, L. Simonelli, L. Stievano, F. Fauth, M. Ménétrier, D. Carlier, C. Masquelier, L. Croguennec, V^{IV} Disproportionation Upon Sodium Extraction From $\text{Na}_3\text{V}_2(\text{PO}_4)_2\text{F}_3$ Observed by Operando X-ray Absorption Spectroscopy and Solid-State NMR, *J. Phys. Chem. C* 121 (2017) 4103–4111.

- [29] E. Boivin, R. David, J.-N. Chotard, T. Bamine, A. Iadecola, L. Bourgeois, E. Suard, F. Fauth, D. Carlier, C. Masquelier, L. Croguennec, $\text{LiVPO}_4\text{F}_{1-y}\text{O}_y$ Tavorite-Type Compositions: Influence of the Concentration of Vanadyl-Type Defects on the Structure and Electrochemical Performance, *Chem. Mater.* 30 (2018) 5682–5693.
- [30] A.A. Tsirlin, R. Nath, A.M. Abakumov, Y. Furukawa, D.C. Johnston, M. Hemmida, H.A. Krug Von Nidda, A. Loidl, C. Geibel, H. Rosner, Phase separation and frustrated square lattice magnetism of $\text{Na}_{1.5}\text{VOPO}_4\text{F}_{0.5}$, *Phys. Rev. B - Condens. Matter Mater. Phys.* 84 (2011) 2–13.
- [31] M.E. Tuckerman, A. Chandra, D. Marx, Structure and Dynamics of OH^- (aq), *Acc. Chem. Res.* 39 (2006) 151–158.
- [32] P.R. Kumar, Y.H. Jung, C.H. Lim, D.K. Kim, $\text{Na}_3\text{V}_2\text{O}_{2x}(\text{PO}_4)_2\text{F}_{3-2x}$: a stable and high-voltage cathode material for aqueous sodium-ion batteries with high energy density, *J. Mater. Chem. A Mater. Energy Sustain.* 3 (2015) 6271–6275.
- [33] J.-M. Le Meins, M.-P. Crosnier-Lopez, A. Hemon-Ribaud, G. Courbion, Phase Transitions in the $\text{Na}_3\text{M}_2(\text{PO}_4)_2\text{F}_3$ family ($\text{M}=\text{Al}^{3+}, \text{V}^{3+}, \text{Cr}^{3+}, \text{Fe}^{3+}, \text{Ga}^{3+}$): Synthesis, Thermal, Structural, and Magnetic Studies, *J. Solid State Chem.* 148 (1999) 260–277.
- [34] P. Serras, J. Alonso, N. Sharma, J. Miguel, P. Kubiak, M.L. Fdez-Gubieda, T. Rojo, Electrochemical Na Extraction / Insertion of $\text{Na}_3\text{V}_2\text{O}_{2x}(\text{PO}_4)_2\text{F}_{3-2x}$, *Chem. Mater.* 25 (2013) 4917–4925.
- [35] F. Sauvage, E. Quarez, J.M. Tarascon, E. Baudrin, Crystal structure and electrochemical properties vs. Na^+ of the sodium fluorophosphate $\text{Na}_{1.5}\text{VOPO}_4\text{F}_{0.5}$, *Solid State Sci.* 8 (2006) 1215–1221.
- [36] H. Deng, J. Wang, R. Callender, W.J. Ray, Relationship between Bond Stretching Frequencies and Internal Bonding for $[\text{}^{16}\text{O}_4]$ - and $[\text{}^{18}\text{O}_4]$ Phosphates in Aqueous Solution, *J. Phys. Chem. B* 102 (1998) 3617–3623.
- [37] M. Bianchini, F. Fauth, N. Brisset, F. Weill, E. Suard, C. Masquelier, Croguen, Comprehensive Investigation of the $\text{Na}_3\text{V}_2(\text{PO}_4)_2\text{F}_3$ – $\text{NaV}_2(\text{PO}_4)_2\text{F}_3$ System by Operando High Resolution Synchrotron X-ray Diffraction, *Chem. Mater.* 27 (2015) 3009–3020.
- [38] N. Sharma, P. Serras, V. Palomares, H.E.A. Brand, J. Alonso, P. Kubiak, M.L. Fdez-gubieda, T. Rojo, Sodium Distribution and Reaction Mechanisms of a $\text{Na}_3\text{V}_2\text{O}_2(\text{PO}_4)_2\text{F}$ Electrode during Use in a Sodium-Ion Battery, *Chem. Mater.* 26 (2014) 3391–3402.
- [39] G. Yan, S. Mariyappan, G. Rousse, Q. Jacquet, M. Deschamps, R. David, B. Mirvaux, J.W. Freeland, J. Tarascon, Higher energy and safer sodium ion batteries via an electrochemically made disordered $\text{Na}_3\text{V}_2(\text{PO}_4)_2\text{F}_3$ material, *Nat. Commun.* 10 (2019) 585.
- [40] S.T. Dacek, W.D. Richards, D.A. Kitchaev, G. Ceder, Structure and Dynamics of Fluorophosphate Na-Ion Battery Cathodes, *Chem. Mater.* 28 (2016) 5450–5460.
- [41] M. Xu, P. Xiao, S. Stauffer, J. Song, G. Henkelman, J.B. Goodenough, Theoretical and experimental study of vanadium-based fluorophosphate cathodes for rechargeable batteries, *Chem. Mater.* 26 (2014) 3089–3097.
- [42] S. Liu, L. Wang, J. Liu, M. Zhou, Q. Nian, Y. Feng, Z. Tao, L. Shao, $\text{Na}_3\text{V}_2(\text{PO}_4)_2\text{F}_3$ –SWCNT: a high voltage cathode for non-aqueous and aqueous sodium-ion batteries, *J. Mater. Chem. A.* 7 (2019) 248–256.

Table

Table 1: Unit cell parameters of $\text{Na}_3\text{V}_2(\text{PO}_4)_2\text{F}_{3-y'}\text{O}_{y'}$ ($0 \leq y' \leq 2$). For $y' = 1.5$ and $y' = 2.0$, the two unit cells (orthorhombic and tetragonal) could not be discriminated by the Rietveld analysis of the diffraction data.

y' value	Composition	Space group	a (Å)	b (Å)	c (Å)	V/Z (Å³)
0.0	$\text{Na}_3\text{V}_2(\text{PO}_4)_2\text{F}_3$	<i>Amam</i>	9.02847(3)	9.04444(3)	10.74666(6)	219.386(6)
0.2	$\text{Na}_3\text{V}_2(\text{PO}_4)_2\text{F}_{2.8}\text{O}_{0.2}$	<i>Amam</i>	9.0308(1)	9.0429(1)	10.7389(1)	219.248(1)
0.4	$\text{Na}_3\text{V}_2(\text{PO}_4)_2\text{F}_{2.6}\text{O}_{0.4}$	<i>Amam</i>	9.0322(1)	9.0412(1)	10.7213(1)	218.885(1)
0.6	$\text{Na}_3\text{V}_2(\text{PO}_4)_2\text{F}_{2.4}\text{O}_{0.6}$	<i>Amam</i>	9.0336(1)	9.0396(1)	10.7065(1)	218.576(1)
0.8	$\text{Na}_3\text{V}_2(\text{PO}_4)_2\text{F}_{2.2}\text{O}_{0.8}$	<i>Amam</i>	9.0337(1)	9.0383(1)	10.6962(1)	218.337(1)
1.0	$\text{Na}_3\text{V}_2(\text{PO}_4)_2\text{F}_2\text{O}$	<i>Amam</i>	9.0353(1)	9.0375(1)	10.6863(1)	218.151(1)
1.5	$\text{Na}_3\text{V}_2(\text{PO}_4)_2\text{F}_{1.5}\text{O}_{1.5}$	<i>P4₂/mmm</i>	9.0291(2)	9.0291(2)	10.6375(5)	216.803(3)
2.0	$\text{Na}_3\text{V}_2(\text{PO}_4)_2\text{FO}_2$	<i>P4₂/mmm</i>	9.0287(9)	9.0287(9)	10.6056(1)	216.132(2)

Figure captions

Figure 1: Top: TGA-MS results recorded for a mixture of $(2\text{VPO}_4 + 3\text{NaF})$ heated at $5^\circ\text{C}\cdot\text{min}^{-1}$ between 25°C and 650°C . Fluorine was the only gas released, from 450°C ; Bottom: TGA-MS results recorded for a mixture of $(\text{VPO}_4 + \text{VOPO}_4 + 2\text{NaF} + \frac{1}{2} \text{Na}_2\text{CO}_3)$ heated at $5^\circ\text{C}\cdot\text{min}^{-1}$ between 25°C and 500°C . No O_2 evolution was detected. CO_2 was the main gas released during the reaction process. Minor loss of Fluorine (not shown) was also observed (Ion current below $2 \cdot 10^{-9}$).

Figure 2: (a) Powder XRD patterns of $\text{Na}_3(\text{VO})_2(\text{PO}_4)_2\text{F}$, collected before and after washing, on a $\text{Cu K}\alpha_{1,2}$ diffractometer. The impurities highlighted by * are $\text{Na}(\text{PO}_3)_3$ and $\text{Na}_2\text{V}_2\text{O}_5$. (b) ^{31}P ss-NMR spectra collected for $\text{Na}_3(\text{VO})_2(\text{PO}_4)_2\text{F}$ before and after washing. The spectra were recorded at 100 MHz (MAS = 30 kHz). (c) IR spectra of unwashed and washed $\text{Na}_3(\text{VO})_2(\text{PO}_4)_2\text{F}$ powders in the wavenumber range of $400 - 4000 \text{ cm}^{-1}$. (d) Comparison of the IR spectra of $\text{Na}_3\text{V}_2(\text{PO}_4)_2\text{F}_3$, $\text{Na}_3\text{V}_2(\text{PO}_4)_2\text{F}_{2.4}\text{O}_{0.6}$, $\text{Na}_3\text{V}_2(\text{PO}_4)_2\text{F}_2\text{O}$, $\text{Na}_3\text{V}_2(\text{PO}_4)_2\text{F}_{1.5}\text{O}_{1.5}$, and $\text{Na}_3(\text{VO})_2(\text{PO}_4)_2\text{F}$ powders recovered after washing in the wavenumber range of $800 - 1300 \text{ cm}^{-1}$.

Figure 3: The evolution of the unit cell parameters determined for $\text{Na}_3\text{V}_2(\text{PO}_4)_2\text{F}_{3-y'}\text{O}_{y'}$ ($0 \leq y' \leq 2$) materials obtained in our group (in this work, and by Broux et al. [14]), in comparison with those reported in the literature [7,13,30]. All the $\text{Na}_3\text{V}_2(\text{PO}_4)_2\text{F}_{3-y'}\text{O}_{y'}$ phases reported in the literature were indexed in the space group $P4_2/mnm$. By the use of high resolution synchrotron X-ray powder diffraction, a subtle orthorhombic distortion described in the space group $Amam$ was detected in the phases such as $y' \leq 1$.

Figure 4: (Top) Rietveld refinement of synchrotron powder X-ray diffraction of $\text{Na}_3(\text{VO})_2(\text{PO}_4)_2\text{F}$ (after washing) recorded at $\lambda = 0.8251 \text{ \AA}$ in the $Amam$ space group. The zooms on the figure show the presence of some low intensity diffraction peaks that are not indexed; (Bottom) The refinement of synchrotron powder X-ray diffraction of $\text{Na}_3(\text{VO})_2(\text{PO}_4)_2\text{F}$ refined in the $P2_1/m$ space group with a vector of modulation $q = \frac{1}{2} b^* + \frac{1}{2} c^*$.

Figure 5: (Left) Comparison of the electrochemical charge/discharge curves obtained for the carbon-coated $\text{Na}_3\text{V}_2(\text{PO}_4)_2\text{F}_3$, $\text{Na}_3\text{V}_2(\text{PO}_4)_2\text{F}_2\text{O}$, $\text{Na}_3\text{V}_2(\text{PO}_4)_2\text{F}_{1.5}\text{O}_{1.5}$ and $\text{Na}_3(\text{VO})_2(\text{PO}_4)_2\text{F}$ in half sodium cells at the cycling rate of C/10 per Na^+ ion; (Right) The first derivatives of the corresponding electrochemical curves.

Figure 6: (a) The electrochemical profile recorded for the half cell $\text{Na}/\text{Na}_3\text{V}_2(\text{PO}_4)_2\text{F}_3$ during the first and the second cycles, the voltage window being widened up to 5.0 V vs. Na^+/Na during the first cycle. The inset gives the corresponding charge/discharge capacities as a function of the cycle number. (b) The corresponding first derivative curves calculated for the first and second cycles Irreversible reaction is highlighted by an arrow. (c) The electrochemical profile recorded for the half cell $\text{Na}/\text{Na}_3\text{V}_2(\text{PO}_4)_2\text{F}_{1.5}\text{O}_{1.5}$ during several cycles, the voltage window being widened up to 5.0 V vs. Na^+/Na during the first cycle. (d) The corresponding first derivative curves.

Figure 7: (a) The correlation between the electrochemical profile and the XANES spectra recorded *operando* during the cycling of the cell $\text{Na}/\text{Na}_3\text{V}_2(\text{PO}_4)_2\text{F}_3$ at C/5 per Na^+ ion. (b) *Operando* Vanadium K edge XANES spectra recorded during Na^+ de-intercalation from $\text{Na}_3\text{V}_2(\text{PO}_4)_2\text{F}_3$. The inset focuses on the pre-edge region. (c) The correlation between the electrochemical profile and the XANES spectra recorded *operando* during the cycling of the cell $\text{Na}/\text{Na}_3\text{V}_2(\text{PO}_4)_2\text{F}_{1.5}\text{O}_{1.5}$ at C/10 per Na^+ ion. (d) *Operando* Vanadium K edge XANES spectra recorded during Na^+ de-intercalation from $\text{Na}_3\text{V}_2(\text{PO}_4)_2\text{F}_{1.5}\text{O}_{1.5}$. The inset focuses on the pre-edge region.

Figure 8: (a) A comparison of the Vanadium K edge XANES spectra recorded for a $\text{Na}/\text{Na}_3\text{V}_2(\text{PO}_4)_2\text{F}_3$ half-cell at some significant states of charge: beginning of the charge (Spectrum #1), at the end of the first plateau on charge (Spectrum #20), at the end of the second plateau on charge (Spectrum #40), and at the end of the third plateau on charge (Spectrum #57). (b) A comparison of the Vanadium K edge XANES spectra recorded on a $\text{Na}/\text{Na}_3\text{V}_2(\text{PO}_4)_2\text{F}_{1.5}\text{O}_{1.5}$ half-cell at some significant states of charge: beginning of the charge (Spectrum #1), formation of $\text{Na}_2\text{V}_2(\text{PO}_4)_2\text{F}_{1.5}\text{O}_{1.5}$ (Spectrum #35), formation of $\text{Na}_1\text{V}_2(\text{PO}_4)_2\text{F}_{1.5}\text{O}_{1.5}$ (Spectrum #70), and at the end of the charge (Spectrum #83). The spectra #71 and #83 are very similar as there is no change in the Vanadium oxidation state and in its local environment.